Environmental Science and Pollution Research, Vol. 24, Issue 14, May 2017, pp. 12589-12598
DOI:10.1007/s11356-016-7564-6

Environmental Science and Pollution Research

Magnetically Recoverable TiO_2-WO_3 Photocatalyst to Oxidize Bisphenol A from Model Wastewater under Simulated Solar Light

S. Dominguez[1], M. Huebra[2], C. Han[3], P. Campo[4], M.N. Nadagouda[5], M.J. Rivero[1], I. Ortiz[1*], D.D. Dionysiou[3]

(1) Department of Chemical and Biomolecular Engineering, University of Cantabria, 39005, Santander, Spain, * inmaculada.ortiz@unican.es

(2) Dpto Química Analítica, Universidad País Vasco, 48080, Bilbao, Spain

(3) Environmental Engineering and Science Program, University of Cincinnati, Cincinnati, OH 45221-0012, USA

(4) Cranfield Water Science Institute, Cranfield University, Cranfield, Beds, MK43 0AL, UK

(5) Department of Mechanical and Materials Engineering, Wright State University, Dayton, OH 45324, USA

Acknowledgements

Financial support from the Spanish Ministry of Economy and Competitiveness and from FEDER funds (projects CTM2012-33917, CTM2015-69845-R and CTQ2015-66078-R) are gratefully acknowledged (MINECO/FEDER, UE). Sara Dominguez also thanks the FPI postgraduate research grant (BES-2013-064055) and the predoctoral mobility aid for conducting short stays in R&D Centers (EEBB-I-15-09465).

Abstract

A novel magnetically recoverable, visible light active TiO_2-WO_3 composite (Fe_3O_4@SiO_2@TiO_2-WO_3) was prepared to enable the photocatalyst recovery after the degradation of bisphenol A (BPA) under simulated solar light. For comparison, the photocatalytic activity of other materials such as non-magnetic TiO_2-WO_3, Fe_3O_4@SiO_2@TiO_2, TiO_2 and the commercial TiO_2 P25 was also evaluated under the studied experimental conditions. The structure and morphology of the synthesized materials were characterized by X-ray diffraction (XRD), ~~S~~scanning electron microscopy (SEM), high-resolution transmission electron microscopy (HR-TEM) and electron dispersion spectroscop~~e~~y (EDS). Moreover, Brunauer–Emmett–Teller (BET) surface area and magnetic properties of the samples were determined. The Fe_3O_4@SiO_2@TiO_2-WO_3 and TiO_2-WO_3 led to a BPA degradation of 1~~8~~7.50% and 2~~8~~7.92%, respectively, after 2 h of the simulated solar light irradiation. Even though their activity was lower than that of P25, which degraded completely BPA after 1 h, our catalysts were magnetically separable for their further reuse in the treatment. Furthermore, the influence of the water matrix in the photocatalytic activity of the samples was studied in municipal wastewater. Finally, the identification of reaction intermediates was performed and a possible BPA degradation pathway was proposed to provide a better understanding of the degradation process.

Keywords

Bisphenol A (BPA); degradation pathway; magnetic composite; photocatalysis; TiO_2; WO_3.

Introduction

Contaminants of emerging concern (CECs), including personal care products, pharmaceuticals, disinfectants, pesticides, industrial compounds, fragrances, preservatives and additives, have attracted increasing attention over the last few years owing to their fate and occurrence in the environment and their adverse ecological and human health effects (Barbosa et al., 2016; Fagan et al., 2016).

Bisphenol A (BPA), which is a representative CEC, is a synthetic monomer commonly employed in the manufacture of plastics such as polycarbonates or epoxy resins. It is widely used in plastic bottles, food and beverage containers, dental sealants, adhesives and sheathing of electrical parts (Chiang et al., 2004; Daskalaki et al., 2011). According to the estimation of the United States Environmental Protection Agency (US EPA), over 1 million pounds of BPA leach~~es~~ into the environment annually and it is

frequently found in municipal wastewater treatment plants (WWTPs) (Melcer and Klečka, 2011; Rodríguez et al., 2010; Seachrist et al., 2016). Moreover, BPA is considered an endocrine disrupting compound (EDC) because it may interfere with the endocrine system of several living beings (Sin et al., 2012). Since its low biodegradability hinders its removal via biological treatments, an effective treatment for BPA is required and new alternatives have to be addressed to protect the health of humans and the ecosystem from the pollutant (Rivero et al., 2014).

Advanced oxidation processes (AOPs) are technologies based on the generation of strongly reactive oxygen species such as hydroxyl radicals ($^{\bullet}OH$) (Dominguez et al., 2015; Rioja et al., 2014). ~~AOPs are~~ The application of these methods is a promising alternative for the degradation of different recalcitrant organic contaminants (Fernández-Castro et al., 2015). Among AOPs, photocatalysis is an attractive technology because it operates at environment temperature and pressure and avoids secondary pollution. Additionally, it has shown positive results in BPA mineralization (Colombo et al., 2012; Dimitroula et al. 2012).

Due to its photostability, relatively high photocatalytic activity, nontoxicity and low cost, TiO_2 has been the most widely used photocatalyst so far (Dominguez et al., 2015). Nevertheless, TiO_2 recovery remains a challenge and limits its application when it is used in powder form (Rashid et al., 2015; Shan et al., 2009). Alternatively, TiO_2 immobilization to an inert support has been proposed. However, this approach reduces the amount of catalyst active sites, decreasing the photocatalytic effectiveness of these materials ~~when~~ compared ~~with~~ to the unsupported photocatalysts (Gaya and Abdullah, 2008). Hence, the development of photocatalysts with properties that facilitate their separation and recovery from treated waters is an interesting scientific and technical challenge; in this field, ~~photacalysts~~ photocatalysts with magnetically recoverable properties appear advantageous (Gómez-Pastora et al., 2016). These materials can be easily separated from the reaction media by external magnetic fields, which facilitates their reuse.

Another critical issue is the lack of TiO_2 activity under visible light illumination owing to its large band gap (3.20 eV for anatase) (Bai et al., 2015; Han et al., 2011; Kou et al., 2015). Thus, several strategies have been adopted to develop effective solar driven TiO_2 photocatalys~~t~~is for practical applications. One of the most suitable solutions is the incorporation of additional components into the TiO_2 structure. ~~Doping the~~ TiO_2 doping with metallic elements, including noble metals such as Au, Pd and Ag, or post-transition metals like Al, Bi and Pb, has been reported (Chen et al., 2015; Daghrir et al., 2013; Han et al., 2014). An ~~A~~alternative solution~~s~~ ~~are~~ is the use of non-metal~~s~~ elements, being the most employed C, F and N, or

coupling TiO_2 with other semiconductors with narrow band gaps, such as Bi_2S_3, WO_3 and ZnO (Daghrir et al., 2013; Dozzi et al., 2014; Pelaez et al., 2012; Zhang et al., 2012; Zhang et al., 2013). Since WO_3 shows a suitable conduction band gap (2.80 eV) for visible light absorption, increasing attention has been paid to the formation of TiO_2-WO_3 composites (Daghrir et al., 2013; Ramos-Delgado et al., 2013). These materials also prevent the fast recombination of the formed electron/holes pairs during the photocatalysis (Daghrir et al., 2013). Moreover, WO_3 is more acidic than TiO_2, which enables the adsorption of hydroxyl radicals and organic pollutants in the surface of the photocatalyst (Gao et al., 2006; Prabhu et al., 2014).

In this paper, magnetically recoverable TiO_2-WO_3, visible light active photocatalysts ~~active under visible light~~ were synthesized and characterized. Their photocatalytic activity on BPA ~~mineralization~~ degradation was evaluated under simulated solar radiation and compared to that of P25, a commercial TiO_2 photocatalyst. Two aqueous matrices such as Milli-Q grade water and wastewater from the City of Cincinnati (OH, USA) were used in the evaluation of the photocatalytic removal of BPA. Furthermore, a degradation mechanism was proposed on the grounds of the identified reaction intermediates.

Materials and methods

Photocatalyst synthesis

Magnetic iron-based nanoparticles were first prepared in 1 liter round bottom flask reactor by adding 600 mL of a mixture of ethanol, Milli-Q grade water and the natural surfactant Muscle 6013 (Verutek) (45:50:5 v/v), 16.70 g of ferrous sulfate heptahydrate (0.10 M $FeSO_4 \cdot 7H_2O$, ACROS Organics), 29.40 g of ferric sulfate pentahydrate (0.20 M $Fe_2(SO_4)_3 \cdot 5H_2O$, ACROS Organics) and 75 mL of ammonium hydroxide (NH_4OH~~)~~, **20**-22%, ~~(~~Fisher Scientific) dropwise until reaching a pH of 10. The reaction continued for 1 h at 60 °C under stirring.

A silica (SiO_2) layer was coated on the obtained magnetic Fe_3O_4 cores to prevent their oxidation according to the modified Stöber method by hydrolysis and condensation of tetraethyl orthosilicate (TEOS, Sigma-Aldrich) (Saiz et al., 2013). ~~Then,~~ Briefly, 1.00 g of ~~C~~cetyl ~~T~~trimethyl ~~A~~ammonium ~~B~~bromide (CTAB, Sigma-Aldrich) and 30 mL of the ferrofluid containing the magnetic Fe_3O_4 cores were dispersed in a reaction media with Milli-Q grade water and ethanol (94:6, v/v) at 60 °C. Then, 5 mL of ~~tetraethyl orthosilicate (~~TEOS~~)~~ were added dropwise to the suspension and the mixture was stirred for 2 h. The obtained precipitate was washed with ethanol, dried at 90 ºC for 12 h, calcined at 450 °C for 18 h and finally grinded.

For the synthesis of the external TiO_2-WO_3 layer, a sol-gel method was used. In this case, 0.50 g of the previously prepared Fe_3O_4@SiO_2 nanoparticles were dispersed in 100 mL of isopropanol (GFS Chemicals) at 80 °C. Titanium isopropoxide (TTIP, ACROS Organics), as a Ti precursor, and an aqueous solution of ammonium tungstate (Sigma-Aldrich), as a tungsten precursor, were added dropwise at the same time and then the solution was kept at 80 °C for 24 h. Therefore, the ~~hydrolysis~~ reactions of both precursors ~~occurred simultaneously~~ started at the same time. Several molar ratios of WO_3 to TiO_2 were evaluated and 15% was selected as optimum. Therefore, this molar ratio was used in the TiO_2-WO_3 photocatalysts tested in the present work. The obtained product was washed with ethanol, dried at 90 °C for 12 h, calcined at 450 °C for 8 h and grinded. In the case of the TiO_2 and Fe_3O_4@SiO_2@TiO_2 photocatalysts, Milli-Q grade water was added dropwise at the same time along with TTIP to facilitate its hydrolysis.

Photocatalyst characterization

The crystalline size and phases of the prepared photocatalysts were determined by X-ray diffraction (XRD) with a X'Pert PRO (Philips) with CuKα radiation source (λ = 1.54 Å) operating at 45 kV and 40 mA. The synthesized photocatalysts morphology was characterized with a JSM-6490LV scanning electron microscope (SEM, JEOL) and with a JEM-2010F (JEOL) high-resolution transmission electron microscope (HR-TEM) with a field emission gun at 200 kV. Electron dispersion spectroscopy (EDS) installed in SEM was employed to observe the chemical composition of the samples. The specific surface area of the nanoparticles was calculated by the Brunauer–Emmett–Teller (BET) method from the nitrogen adsorption-desorption isotherm data employing an ASAP 2000 surface area analyzer (Micromeritics). Magnetization measurements were performed on a Quantum Design MPMS (SQUID) magnetometer at 300 K in the magnetic field range of -50 to 50 kOe.

Photocatalytic experiments

The BPA used in this study was purchased from Sigma-Aldrich. The commercial TiO_2 photocatalyst used was AEROXIDE P25 (Evonik Industries). In this experiment, 100 mL of a 10.00 mg L^{-1} BPA solution were mixed with 0.50 g L^{-1} of the photocatalyst and kept for 24 h premixing in the dark to reach adsorption equilibrium. The photocatalyst loading was selected based on ~~previous studies~~ preliminary laboratory tests. The reactor was mechanically stirred using KS 130 stirrer~~,~~ (IKA) in order to ensure

uniform mixture and to prevent the photocatalyst settling. The solution was irradiated with a 500 W solar simulator (Xenon lamp 67005, Newport Corporation). At given time intervals, the suspension was sampled and filtered through a 0.20 μm Mini-UniPrep filter (GE Healthcare Life Sciences) prior to analysis. The experiments were carried out in duplicate.

BPA concentration was measured by an Agilent Series 1100 high performance liquid chromatograph (HPLC, Agilent Technologies) with a X Terra MS C18 5 μm (4.60 x 250 mm) analytical column (Waters). The mobile phase used was a mixed solvent of acetonitrile (Fisher Scientific) and Milli-Q grade water (50/50, v/v) with a flow rate of 1 mL min^{-1}. Identification of reaction intermediates by accurate mass measurement was carried out with an Agilent 1900 ~~L~~liquid ~~C~~chromatograph with an Agilent 6540 ~~Q~~quadrupole-~~T~~time of ~~F~~flight/mass spectrometer (LC-Q-TOF/MS). Nitrogen was used as drying gas at a flow rate of 7 L min^{-1} at 300 °C and as sheath gas with a flow rate of 8 L min^{-1} at 250 °C.

Results and discussion

Photocatalyst characterization

The XRD spectra of the photocatalysts samples are shown in Fig. 1. The strongest reflection for anatase was observed at 25.27º (101 plane). Furthermore, anatase showed other primary diffraction peaks with lower intensity at 27.04º, 37.98º, 48.01º, 54.24º, 55.19º, 62.74º, 69.96º, 74.94º and 82.80º, which can be indexed as (110), (004), (200), (105), (211), (204), (220), (215) and (224) planes, respectively (JCPDS No. 21-1272). Signals corresponding to the primary reflections of monoclinic WO_3 were observed at 23.11º, 23.67º, 24.23º and 33.85º, corresponding to the phases (002), (020), (200) and (202), respectively (JCPDS No. 43-1035). For magnetite, the (311) plane showed the strongest peak at ~~43.05º~~ 35.62º. Moreover, other signals were observed at 30.10º, 43.05º, 53.39º, 56.94º and 62.52º, corresponding to the magnetite phases (220), (400), (422), (511) and (440) (JCPDS No. 19-0629).

Fig. 1

Fig. 1 XRD spectra of Fe_3O_4, Fe_3O_4@SiO_2@TiO_2, Fe_3O_4@SiO_2@TiO_2-WO_3, TiO_2 and TiO_2-WO_3 nanoparticles

Images of SEM and HR-TEM analyses show the structural properties of synthesized materials (Fig. 2). As seen in Fig. 2a1, prepared primary Fe_3O_4 nanoparticles as cores of magnetic photocatalysts were

spherical and their average diameter was 23 nm. Cores with similar size were obtained in literature; for instance, Jing et al. (2013) synthesized Fe_3O_4 nanoparticles of 17 nm. However, as shown in Fig. 2b1, the magnetic Fe_3O_4 cores were aggregated and formed large clusters. When the next layer was added, amorphous SiO_2 covered completely the magnetic Fe_3O_4 cores, as seen in Fig. 2a2 and 2b2. After addition of TiO_2, crystalized nanoparticles on the surface of Fe_3O_4@SiO_2 samples were formed, as shown in Fig. 2a3. The TiO_2 nanoparticles covered the whole area of Fe_3O_4@SiO_2 (Fig. 2b3). Similar nanoparticles are shown in Fig. 2a5, confirming that TiO_2 nanoparticles were effectively deposited on the surface of Fe_3O_4@SiO_2. Nevertheless, when WO_3 was added to the Fe_3O_4@SiO_2@TiO_2 interesting ring like structures (Fig. 2a4) and micro-rods (Fig. 2b4) were also observed.

Fig. 2

Fig. 2 Electronic microscopy characterization. HR-TEM images of a1). Fe_3O_4, a2). Fe_3O_4@SiO_2, a3). Fe_3O_4@SiO_2@TiO_2, a4). Fe_3O_4@SiO_2@TiO_2-WO_3, a5). TiO_2 and a6). TiO_2-WO_3 nanoparticles. SEM images of b1). Fe_3O_4, b2). Fe_3O_4@SiO_2, b3). Fe_3O_4@SiO_2@TiO_2, b4). Fe_3O_4@SiO_2@TiO_2-WO_3 b5). TiO_2 and b6). TiO_2-WO_3 nanoparticles

To verify the existence of W and Ti elements in the Fe_3O_4@SiO_2@TiO_2-WO_3 photocatalyst and the average molar ratio of WO_3 to TiO_2, a qualitative analysis of elemental compositions was performed by EDS (Fig. 3). The apparition of signals ascribed to Ti and W confirmed the formation of the external layer of the composite. The molar content of WO_3, calculated from the weight content, was found to be 16 %, which ~~is~~ was close to the theoretical value (15%). Si and Fe elements were detected, indicating that not all the SiO_2 interlayer was etched off.

Fig. 3

Fig. 3 EDS spectrum of the Fe_3O_4@SiO_2@TiO_2-WO_3 photocatalyst

The magnetic properties of the synthesized nanoparticles were characterized through the determination of the magnetization curves shown in Fig. 4. The magnetization saturation (M_s) of the samples was determined at 300 K for the evaluation of the magnetic response to an external field (H). Fe_3O_4 and Fe_3O_4@SiO_2@TiO_2 presented M_s values of 68.13 and ~~15.9~~ 16.00 emu g^{-1}, respectively. Therefore, after

adding SiO_2 and TiO_2 layers~~,~~ a substantial decrease in the magnetic properties of the samples was observed. This behaviour was also detected by Chi et al. (2013), who prepared Fe_3O_4 and Fe_3O_4@SiO_2@TiO_2 with a M_s of 79.90 and 33.50 emu g^{-1}, respectively; and by Jing et al. (2013), who synthesized ~~Fe_3O_4 and~~ Fe_3O_4@TiO_2 nanoparticles with a M_s below ~~50~~ 46.60 emu g^{-1}. Furthermore, the Fe_3O_4@SiO_2@TiO_2-WO_3 exhibited a slightly smaller Ms value than the Fe_3O_4@SiO_2@TiO_2 nanocomposite, 8.54 emu g^{-1}, which could be attributed to an increase in the mass and size caused by the addition of WO_3. It has to be pointed out that the M_s of the photocatalysts ~~is~~ was still strong enough to allow their magnetic recovery after the photocatalytic process. Moreover, the coercivity and remanent magnetization value ~~are~~ were close to zero, indicating that they showed superparamagnetic behaviour (Fisli et al. 2013).

Fig. 4

Fig. 4 Magnetization curves of Fe_3O_4, Fe_3O_4@SiO_2@TiO_2 and Fe_3O_4@SiO_2@TiO_2-WO_3 samples

BET surface area and the nitrogen adsorption–desorption isotherms were ~~studied~~ determined for the photocatalysts. In all the cases, according to the IUPAC classification, the isotherms were type IV with H3 hysteresis, showing the mesoporous nature of the solids. The commercial TiO_2 P25 surface area was found to be 56.48 ± 0.33 m^2 g^{-1}, value that is consistent with those reported in the literature (Lucas et al., 2013; Ye et al., 2010). TiO_2, TiO_2-WO_3, Fe_3O_4@SiO_2@TiO_2 and Fe_3O_4@SiO_2@TiO_2-WO_3 particles showed a similar increase in the surface area with respect to the commercial TiO_2 P25 solid, with 130.07 ± 0.20, 118.85 ± 0.27, 134.46 ± 0.56 and 115.80 ± 0.27 m^2 g^{-1}, respectively. ~~These larger surface areas could be due to the formation of aggregates (Lucas et al., 2013), in agreement with SEM and HR-TEM results.~~ Interestingly, the BET surface area decreased by adding different material coating layers or nanoparticles. It seems that the formed nanoparticles at the outer layer may deposit on and block the pores of the previously prepared cores.

Photocatalyst activity

Figure 5 shows the photocatalytic treatment of BPA in Milli-Q grade water. As depicted, ~~without photocatalyst~~ in the absence of photocatalyst there was not BPA oxidation, indicating that BPA is very stable under simulated solar light irradiation. After 1 h of treatment with the TiO_2 P25 photocatalyst, ~~the~~

BPA was completely ~~eliminated~~ degraded. However, using the Fe_3O_4@SiO_2@TiO_2-WO_3 composite only 1~~8~~7.50% ± 0.01% BPA was removed after 2 h of treatment. This behavior may be due to the small amount of TiO_2-WO_3 in the outer layer of the composite particles, which provides the photocatalytic capacity. Unfortunately, it was not possible to determine the amount of TiO_2-WO_3 deposited on the magnetic cores. Eventually, less amount of active photocatalyst was used in the magnetic composites, resulting in much lower BPA degradation rate, compared to P25. For the TiO_2-WO_3 photocatalyst, the performance was slightly better, reaching 2~~8~~7.92% ± 0.71% of BPA ~~elimination~~ oxidation after 2 h. Nevertheless, its activity remained below that shown by the commercial photocatalyst. In the case of the photocatalyst synthesized without WO_3, the magnetic composite removed 4~~1~~0.86% ± 6.24% of BPA at the end of the treatment while the as-prepared non-magnetic one attained a removal of ~~approximately~~ 38.25% ± 5.86%.

Fig. 5

Fig. 5 Photocatalytic removal of BPA with time in Milli-Q water. $[BPA]_0$ = 10.00 mg L^{-1}, [photocatalyst] = 0.50 g L^{-1}. Blank: ◆, TiO_2 P25: ×, TiO_2: ✳, TiO_2-WO_3: ▲, Fe_3O_4@SiO_2@TiO_2: ●, Fe_3O_4@SiO_2@TiO_2-WO_3: ■.

Table 1 shows the pseudo-first order kinetic constants (k), standard deviations (σ) and regression coefficients (R^2) obtained from the fitting of the experimental data to a pseudo-first order kinetic model (Eq. 1). The data corresponding to the commercial TiO_2 P25 fitted properly to the proposed kinetic equation, with a ~~value of the pseudo-first order kinetic constant~~ k of 5.12~~1~~ x 10^{-2} min^{-1}, σ of 1.98 x 10^{-3} min^{-1} and R^2 of 0.9~~76~~8. The lower values of the regression coefficients obtained for the composites are attributed to the low degradation rates under the studied experimental conditions.

$$\frac{-\,d\,[BPA]}{dt} = k \cdot [BPA] \quad (1)$$

[BPA] is the concentration of bisphenol A (mg L^{-1}), t is the reaction time (min) and k is the pseudo-first order kinetic constant (min^{-1}).

Table 1 Pseudo-first order k~~K~~inetic constants of the photocatalytic treatment of the Milli-Q water. $[BPA]_0$ = 10.00 mg L^{-1}, [photocatalyst] = 0.50 g L^{-1}

	TiO_2 P25	TiO_2	TiO_2-WO_3	Fe_3O_4@SiO_2@TiO_2	Fe_3O_4@SiO_2@TiO_2-WO_3
k (min^{-1})	5.12~~1~~ x 10^{-2}	0.3~~88~~9 x 10^{-2}	0.31~~1~~ x 10^{-2}	0.39~~1~~ x 10^{-2}	0.14~~4~~ x 10^{-2}
σ (min^{-1})	1.98 x 10^{-3}	0.48 x 10^{-3}	0.45 x 10^{-3}	0.49 x 10^{-3}	0.04 x 10^{-3}
R^2	0.97~~6~~8	0.89~~0~~	0.92~~4~~	0.90~~9~~1	0.~~799~~80

Next, the photocatalytic treatment of BPA in the wastewater generated at the University of Cincinnati was carried out under the same experimental conditions as in the case of Milli-Q water (Fig. 6). The average alkalinity was 292.00 mg $CaCO_3$ L^{-1} and the average dissolved organic carbon content was 23.~~6~~59 mg L^{-1} but BPA was not detected; therefore, 10.00 mg L^{-1} of BPA were spiked. Since this effluent is a much more complex matrix that contains numerous substances, the photocatalytic efficiency of the photocatalysts might be much smaller than that of Milli-Q water. The TiO_2 P25 removed 6~~3~~2.77% ± 1.57% of BPA in 3 h, being the degradation rate lower than in the Milli-Q water, where complete removal was achieved after 1 h of treatment. This similar behavior also occurred when using the TiO_2-WO_3 composite, ~~and~~ with the observed photocatalytic activity ~~was~~ being negligible. The lower activity achieved with both photocatalysts could be attributed to the existence of inorganic ions, such as carbonates, or dissolved organic matter that can provoke an inhibitory effect. They may compete with the target pollutants for the adsorption sites on the TiO_2 surface and/or act as $^{\bullet}OH/h^{+}$ scavengers, generating less powerful oxidants (Carbajo et al., 2014). Pelaez et al. (2011) also reported the scavenging effects of carbonates to degrade water contaminants during TiO_2 photocatalysis.

Again the experimental data of the BPA degradation when using TiO_2 P25 were fitted to a pseudo-first order kinetic model. The kinetic constant obtained was 0.53~~0~~ x 10^{-2} min^{-1} (σ = 0.41 x 10^{-3} min^{-1}, R^2 = 0.99~~2~~), being approximately 10 fold smaller than that estimated for the BPA degradation in Milli-Q water.

Fig. 6

Fig. 6 Photocatalytic removal of BPA with time in wastewater. $[BPA]_0$ = 10.00 mg L^{-1}, [photocatalyst] = 0.50 g L^{-1}. TiO_2 P25: ×, TiO_2-WO_3: ▲.

Bisphenol A degradation pathway

During the photocatalytic treatment of BPA in Milli-Q grade water the formation of numerous intermediate compounds was noticed. The peak corresponding to BPA ~~progressively~~ decreased

progressively ~~over~~ with time, other ~~features~~ peaks representing intermediate products appeared and disappeared, and ~~a few~~ some signals corresponding to the final products showed up. In this work, a degradation pathway is proposed. The generated $^{\bullet}OH$ attack the BPA molecule, which is transformed into compounds with different extent of hydroxylation ~~degrees.~~; ~~it~~ BPA is decomposed in intermediate compounds with one aromatic ring through the formation of phenyl and isopropylphenol radicals (Sin et al., 2012; Thiruvenkatachari et al., 2005). When using TiO_2 P25 (Fig. 7), 4-isopropylphenol ($C_9H_{12}O$), 4-hydroxyacetophenone ($C_8H_8O_2$)~~, 4-isopropanol-1,2-benzenediol ($C_9H_{12}O_3$)~~ and 5-hydroxy-2-methylbenzoic acid ($C_8H_8O_3$) were ~~detected~~ formed during the first 5 min and remained at the end of the treatment, as previously reported elsewhere (~~Da Silva et al., 2014;~~ Maroga Mboula et al., 2013; Sharma et al., 2016). The formation of 4-isopropanol-1,2-benzenediol ($C_9H_{12}O_3$) was also observed in the first minutes of reaction and then disappeared, confirming the behavior observed by Da Silva et al. (2014). Furthermore, 2,4,5-trihydroxyacetophenone ($C_8H_8O_4$), which could be formed from the hydroxylation of the 4-hydroxyacetophenone, was also identified within the first 5 min of treatment. However, as seen in Fig. 7, when using any of the photocatalysts synthesized in this work these compounds were not detected. For this case, 2-(4-hydroxyphenyl)-2-propanol ($C_9H_{12}O_2$) was the only ~~intermediate compound~~ aromatic byproduct identified and appeared after 30 min of reaction. Thiruvenkatachari et al. (2005), Tsai et al. (2009) and Watanabe et al. (2003) also found 2-(4-hydroxyphenyl)-2-propanol during the photocatalytic oxidation of BPA but using TiO_2 P25. In a further stage of the reaction, the oxidation of the aromatic ring of the generated intermediate compounds leads to the formation of different organic acids such as maleylacetic ($C_6H_6O_5$) and formic (CH_2O_2) (Ferro Orozco et al., 2016; Thiruvenkatachari et al., 2005; Watanabe et al., 2003). It has to be remarked that acidic compounds with molecular weights of 114.00, 163.00 and 199.00 g mol^{-1} were also observed using both TiO_2 P25 and the synthesized photocatalysts, nevertheless, their assignment to a specific structure was not possible. Finally, these acids could be mineralized to carbon dioxide and water in an ultimate stage.

Fig. 7

Fig. 7 Proposed route for the degradation of BPA. Solid lines: TiO_2 P25, dashed lines: synthesized photocatalysts

Conclusions

A magnetically separable nanocomposite, Fe_3O_4@SiO_2@TiO_2-WO_3, was prepared and characterized. Its photocatalytic activity for the BPA degradation under simulated solar light was studied. Non-magnetic TiO_2-WO_3, Fe_3O_4@SiO_2@TiO_2 and pure TiO_2 were also synthesized for their evaluation. Their photocatalytic activity for BPA degradation was compared to P25 and was studied in both Milli-Q grade water and real wastewater. Due to the complexity of the wastewater chemical composition, the performance of the photocatalysts decreased when compared to Milli-Q grade water. The P25 exhibited a better photocatalytic behaviour compared to the prepared composite photocatalysts but these were magnetically separable and facilitate their removal from the treated water. The analytical identification of reaction intermediates has been carried out. BPA led to intermediate compounds with one aromatic ring, however, when using any of the composites synthesized in this work, 2-(4-hydroxyphenyl)-2-propanol was the only intermediate compound identified and the compounds observed when using P25 were not detected. In a further stage of the reaction, the formation of different organic acids took place; with these results the reaction pathway has been proposed.

Finally, it is worth noticing that although the efficient and low cost magnetic separation of the catalyst is highly desirable for implementation of photocatalytic processes, further work is required to analyze and improve the photocatalytic activity of the synthesized nanocomposites.

References

- Bai S, Liu H, Sun J, Tian Y, Chen S, Song J, Luo R, Li D, Chen A, Liu CC (2015) Improvement of TiO_2 photocatalytic properties under visible light by WO_3/TiO_2 and MoO_3/TiO_2 composites. Appl Surf Sci 338: 61–68. doi: 10.1016/j.apsusc.2015.02.103
- Barbosa MO, Moreira NFF, Ribeiro AR, Pereira MFR, Silva AMT (2016) Occurrence and removal of organic micropollutants: an overview of the watch list of EU Decision 2015/495. Water Res 94: 257–279. doi: 10.1016/j.watres.2016.02.047
- Carbajo J, García-Muñoz P, Tolosana-Moranchel A, Faraldos M, Bahamonde A~~,~~ (2014) Effect of water composition on the photocatalytic removal of pesticides with different TiO_2 catalysts. Environ Sci Pollut Res ~~(2014)~~ 21: 12233–12240. doi: 10.1007/s11356-014-3111-5
- Chen J, Qiu F, Xu W, Cao S, Zhu H (2015) Recent progress in enhancing photocatalytic efficiency of TiO_2-based materials. Appl Catal A: Gen 495: 131–140. doi: 10.1016/j.apcata.2015.02.013

- Chi Y, Yuan Q, Li Y, Zhao L, Li N, Li X, Yan W (2013) Magnetically separable Fe_3O_4@SiO_2@TiO_2-Ag microspheres with well-designed nanostructure and enhanced photocatalytic activity. J Hazard Mater 262: 404–411. doi: 10.1016/j.jhazmat.2013.08.077
- Chiang K, Lim TM , Tsen L, Lee CC (2004) Photocatalytic degradation and mineralization of bisphenol A by TiO_2 and platinized TiO_2. Appl Catal A: Gen 261: 225–237. doi: 10.1016/j.apcata.2003.11.004
- Colombo A, Cappelletti G, Ardizzone S, Biraghi I, Bianchi CL, Meroni D, Pirola C, Spadavecchia F (2012) Bisphenol A endocrine disruptor complete degradation using TiO_2 photocatalysis with ozone. Environ Chem Lett 10:55–60. doi: 10.1007/s10311-011-0328-0
- Da Silva JCC, Teodoro JAR, De Cássia Franco Afonso RJ, Aquino SF, Augusti R (2014) Photodegradation of bisphenol A in aqueous medium: monitoring and identification of by-products by liquid chromatography coupled to high-resolution mass spectrometry. Rapid Commun Mass Spectrom 28: 987–994. doi: 10.1002/rcm.6863
- Daghrir R, Drogui P, Robert D (2013) Modified TiO_2 for environmental photocatalytic applications: a review. Ind Eng Chem Res 52: 3581−3599. doi: 10.1021/ie303468t
- Daskalaki VM, Frontistis Z, Mantzavinos D, Katsaounis (2011) A Solar light-induced degradation of bisphenol-A with TiO_2 immobilized on Ti. Catal Today 161: 110–114. doi: 10.1016/j.cattod.2010.09.018
- Dimitroula H, Daskalaki VM, Frontistis Z, Kondarides DI, Panagiotopoulou P, Xekoukoulotakis NP, Mantzavinos D (2012) Solar photocatalysis for the abatement of emerging micro-contaminants in wastewater: Synthesis, characterization and testing of various TiO_2 samples. Appl Catal B: Environ 117– 118: 283– 291. doi: 10.1016/j.apcatb.2012.01.024
- Dominguez S, Ribao P, Rivero MJ, Ortiz I (2015) Influence of radiation and TiO_2 concentration on the hydroxyl radicals generation in a photocatalytic LED reactor. Application to dodecylbenzenesulfonate degradation. Appl Catal B: Environ 178: 165–169. doi: 10.1016/j.apcatb.2014.09.072
- Dozzi MV, Artiglia L, Granozzi G, Ohtani B, Selli E (2014) Photocatalytic activity vs structural features of titanium dioxide materials singly doped or codoped with fluorine and boron. J Phys Chem C 118: 25579−25589. doi: 10.1021/jp5084696

- Fagan R, McCormack DE, Dionysiou DD, Pillai SC (2016) A review of solar and visible light active TiO_2 photocatalysis for treating bacteria, cyanotoxins and contaminants of emerging concern. Mat Sci Semicon Proc. 42: 2–14. doi: 10.1016/j.mssp.2015.07.052i
- Fernández-Castro P, Vallejo M, San Román MF, Ortiz I (2015) Insight on the fundamentals of advanced oxidation processes. Role and review of the determination methods of reactive oxygen species. J Chem Technol Biotechnol 90: 796–820. doi: 10.1002/jctb.4634
- Ferro Orozco AM, Contreras EM, Zaritzky NE (2016) Biodegradation of bisphenol A and its metabolic intermediates by activated sludge: Stoichiometry and kinetics analysis. Int Biodeter Biodegr 106: 1–9. doi: 10.1016/j.ibiod.2015.10.003
- Fisli A, Saridewi R, Dewi SH, Gunlazuardi J (2013) Preparation and characterization of Fe_3O_4/TiO_2 composites by heteroagglomeration. Adv Mat Res 626: 131–137. doi: 10.4028/www.scientific.net/AMR.626.131
- Gao B, Ma Y, Cao Y, Yang W, Yao J (2006) Great enhancement of photocatalytic activity of nitrogen-doped titania by coupling with tungsten oxide. J Phys Chem B 110: 14391–14397. doi: 10.1021/jp0624606
- Gaya UI, Abdullah AH (2008) Heterogeneous photocatalytic degradation of organic contaminants over titanium dioxide: a review of fundamentals, progress and problems. J Photoch Photobio C 9: 1–12. doi: 10.1016/j.jphotochemrev.2007.12.003
- Gómez-Pastora J, Dominguez S, Bringas E, Rivero MJ, Ortiz I, Dionysiou DD (2016) Review and perspectives on the use of Magnetic Nanophotocatalysts (MNPCs) in water treatment. Chem Eng J. doi:10.1016/j.cej.2016.04.140
- Han C, Likodimos V, Khan JA, Nadagouda MN, Andersen J, Falaras P, Rosales-Lombardi P, Dionysiou DD (2014) UV-Visible light-activated Ag-decorated, monodisperse TiO_2 aggregates for treatment of the pharmaceutical oxytetracycline. Environ Sci Pollut Res 21: 11781–11793. doi: 10.1007/s11356-013-2233-5
- Han C, Pelaez M, Likodimos V, Kontos AG, Falaras P, O'Shea K, Dionysiou DD (2011) Innovative visible light-activated sulfur doped TiO_2 films for water treatment. Appl Catal B: Environ 107 (1-2): 77–87. doi:10.1016/j.apcatb.2011.06.039

- Jing J, Li J, Feng J, Li W, Yu WW (2013) Photodegradation of quinoline in water over magnetically separable Fe_3O_4/TiO_2 composite photocatalysts. Chem Eng J 219: 355–360. doi: 10.1016/j.cej.2012.12.058
- Lucas MS, Tavares PB, Peres JA, Faria JL, Rocha M, Pereira C, Freire C (2013) Photocatalytic degradation of Reactive Black 5 with TiO_2-coated magnetic nanoparticles. Catal Today 209: 116–121. doi: 10.1016/j.cattod.2012.10.024
- Maroga Mboula V, Héquet V, Andrés Y, Pastrana-Martínez LM, Doña-Rodríguez JM, Silva AMT, Falaras P (2013) Photocatalytic degradation of endocrine disruptor compounds under simulated solar light. Water Res 47: 3997–4005. doi: 10.1016/j.watres.2013.01.055
- Melcer H, Klečka G (2011) Treatment of wastewaters containing bisphenol A: state of the science review. Water Environ Res 83(7): 650-666 doi: 10.2175/106143010X12851009156925
- Pelaez M, De la Cruz AA, O'Shea K, Falaras P, Dionysiou DD (2011) Effects of water parameters on the degradation of microcystin-LR under visible light-activated TiO_2 photocatalyst, Water Res 45: 3787–3796. doi: 10.1016/j.watres.2011.04.036
- Pelaez M, Nolan NT, Pillai SC, Seery MK, Falaras P, Kontos AG, Dunlop PSM, Hamilton JWJ, Byrne JA, O'Shea K, Entezari MH, Dionysiou DD (2012) A review on the visible light active titanium dioxide photocatalysts for environmental applications. Appl Catal B: Environ 125: 331–349. doi: 10.1016/j.apcatb.2012.05.036
- Prabhu S, Nithya A, Chandra Mohan S, Jothivenkatachalam K Synthesis (2014) Surface acidity and photocatalytic activity of WO_3/TiO_2 nanocomposites – an overview. Mater Sci Forum 781: 63–78. doi: 10.4028/www.scientific.net/MSF.781.63
- Ramos-Delgado NA, Gracia-Pinilla MA, Maya-Treviño L, Hinojosa-Reyes L, Guzman-Mar JL, Hernández-Ramírez A (2013) Solar photocatalytic activity of TiO_2 modified with WO_3 on the degradation of an organophosphorus pesticide. J Hazard Mater 263P: 36–44. doi: 10.1016/j.jhazmat.2013.07.058
- Rashid J, Barakat MA, Ruzmanova Y, Chianese A (2015) $Fe_3O_4/SiO_2/TiO_2$ nanoparticles for photocatalytic degradation of 2-chlorophenol in simulated wastewater. Environ Sci Pollut Res 22: 3149–3157. doi: 10.1007/s11356-014-3598-9

- Rioja N, Benguria P, Peñas FJ, Zorita S (2014) Competitive removal of pharmaceuticals from environmental waters by adsorption and photocatalytic degradation. Environ Sci Pollut Res 21:11168–11177. doi: 10.1007/s11356-014-2593-5
- Rivero MJ, Alonso E, Dominguez S, Ribao P, Ibañez R, Ortiz I, Irabien A (2014) Kinetic analysis and biodegradability of the Fenton mineralization of bisphenol A. J Chem Technol Biotechnol 89: 1228–1234. doi: 10.1002/jctb.4376
- Rodríguez EM, Fernández G, Klamerth N, Maldonado MI, Álvarez PM, Malato S (2010) Efficiency of different solar advanced oxidation processes on the oxidation of bisphenol A in water. Appl Catal B: Environ 95: 228–237. doi: 10.1016/j.apcatb.2009.12.027
- Saiz J, Bringas E, Ortiz I (2013) Functionalized magnetic nanoparticles as new adsorption materials for arsenic removal from polluted waters. J Chem Technol Biotechnol 89: 909–918. doi: 10.1002/jctb.4331
- Seachrist DD, Bonk KW, Ho SM, Prins G, Sotod AM, Keria RA (2016) A review of the carcinogenic potential of bisphenol A. Reprod Toxicol 59: 167–182. doi: 10.1016/j.reprotox.2015.09.006
- Shan G, Yan S, Tyagi RD, Surampalli RY, Zhang TC (2009) Applications of nanomaterials in environmental science and engineering: a review. Pract Period Hazard Toxic Radioact Waste Manage 13: 110–119. doi: 10.1061/(ASCE)1090-025X(2009)13:2(110)
- Sharma J, Mishra IM, Kumar V (2016) Mechanistic study of photo-oxidation of Bisphenol-A (BPA) with hydrogen peroxide (H_2O_2) and sodium persulfate (SPS). J Environ Manage 166: 12–22. doi: 10.1016/j.jenvman.2015.09.043
- Sin JC, Lam SM, Mohamed AR, Lee KT (2012) Degrading endocrine disrupting chemicals from wastewater by TiO_2 photocatalysis: a review. Int J Photoenergy, 185159. doi: 10.1155/2012/185159
- Thiruvenkatachari R, Kwon TO, Moon IS (2005) Application of slurry type photocatalytic oxidation-submerged hollow fiber microfiltration hybrid system for the degradation of bisphenol A (BPA). Separ Sci and Technol 40: 2871–2888. doi: 10.1080/01496390500333160
- Tsai WT, Lee MK, Su TY, Chang YM (2009) Photodegradation of bisphenol-A in a batch TiO_2 suspension reactor. J Hazard Mater 168: 269–275. doi: 10.1016/j.jhazmat.2009.02.034

- Watanabe N, Horikoshi S, Kawabe H, Sugie Y, Zhao J, Hidaka H (2003) Photodegradation mechanism for bisphenol A at the TiO_2/H_2O interfaces. Chemosphere 52: 851–859. doi: 10.1016/S0045-6535(02)00837-8
- Ye M, Zhang Q, Hu Y, Ge J, Lu Z, He L, Chen Z, Yin Y (2010) Magnetically recoverable core–shell nanocomposites with enhanced photocatalytic activity. Chem Eur J 16: 6243–6250. doi: 1002/chem.200903516
- Zhang YC, Li J, Xu HY (2012) One-step in situ solvothermal synthesis of SnS_2/TiO_2 nanocomposites with high performance in visible light-driven photocatalytic reduction of aqueous Cr(VI). Appl Catal B: Environ 123–124: 18–26. doi: 10.1016/j.apcatb.2012.04.018
- Zhang YC, Yang M, Zhang G, Dionysiou DD (2013) HNO_3-involved one-step low temperature solvothermal synthesis of N-doped TiO_2 nanocrystals for efficient photocatalytic reduction of Cr(VI) in water. Appl Catal B: Environ 142–143: 249–258. doi: 10.1016/j.apcatb.2013.05.023

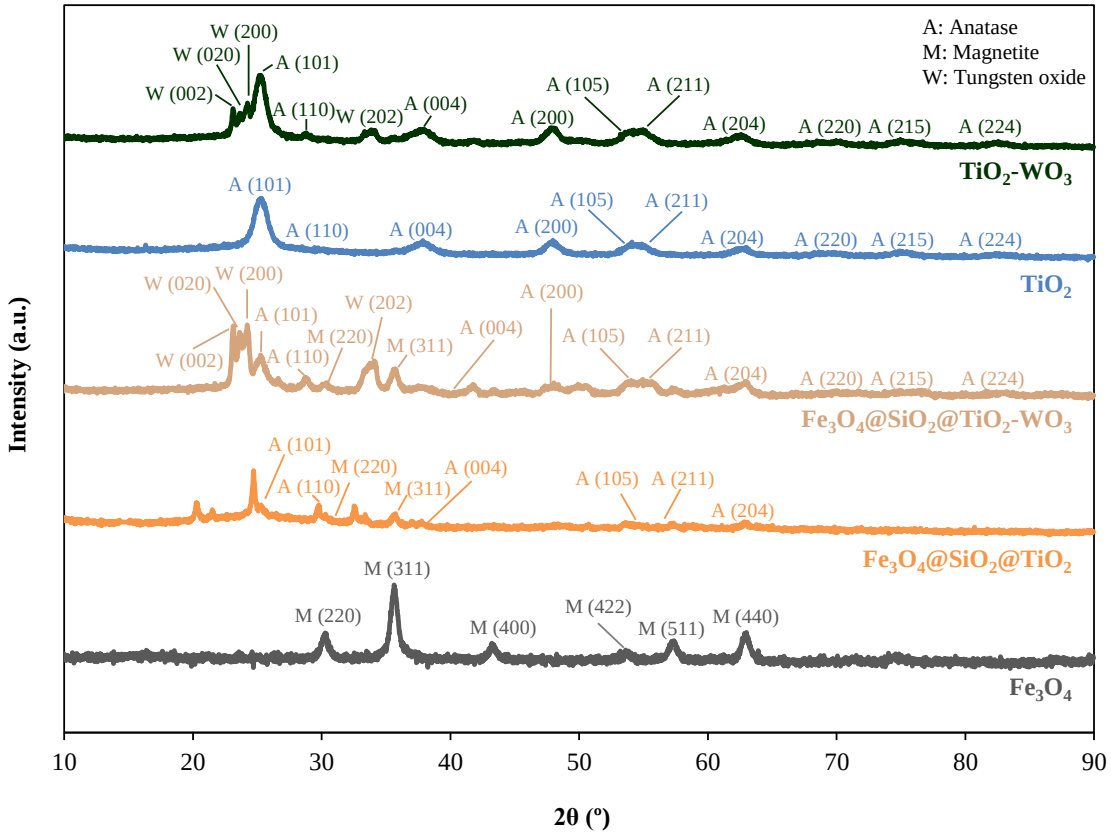
A: Anatase
M: Magnetite
W: Tungsten oxide
W (200)
W (020)
A (101)
W (002)
A (110)
W (202)
A (004)
A (200)
A (105)
A (211)
A (204)
A (220)
A (215)
A (224)
TiO2-WO3
A (101)
A (110)
A (004)
A (200)
A (105)
A (211)
A (204)
A (220)
A (215)
A (224)
TiO2
W (020)
W (200)
A (101)
W (202)
M (220)
M (311)
A (004)
A (200)
A (105)
A (211)
W (002)
A (110)
A (204)
A (220)
A (215)
A (224)
Fe3O4@SiO2@TiO2-WO3
A (101)
M (220)
A (004)
A (110)
M (311)
A (105)
A (211)
A (204)
Fe3O4@SiO2@TiO2
M (311)
M (220)
M (400)
M (422)
M (511)
M (440)
Fe3O4
Intensity (a.u.)
10
20
30
40
50
60
70
80
90
2θ (°)

a1).

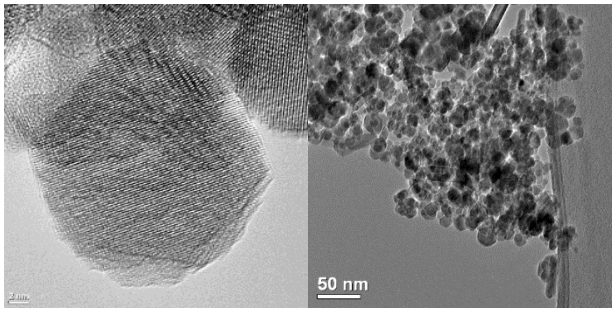

b1).

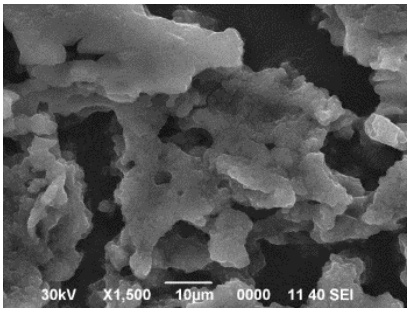

a2).

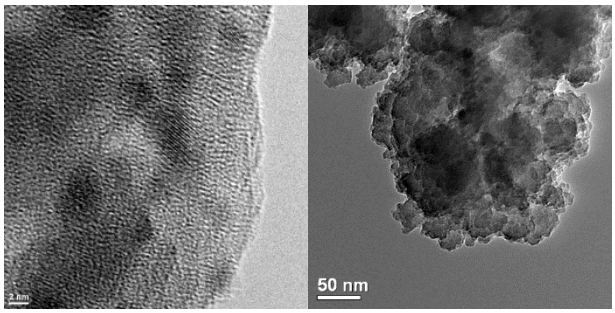

b2).

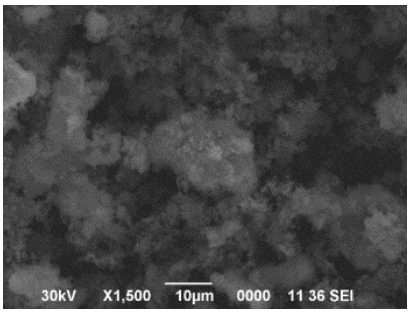

a3).

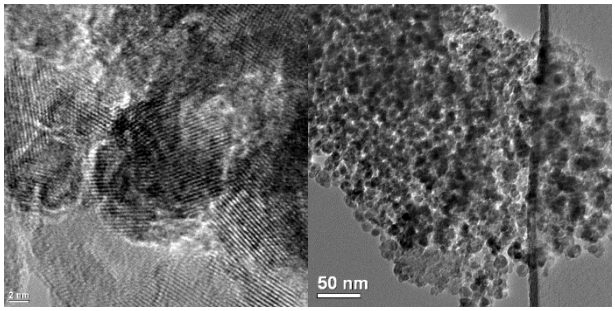

b3).

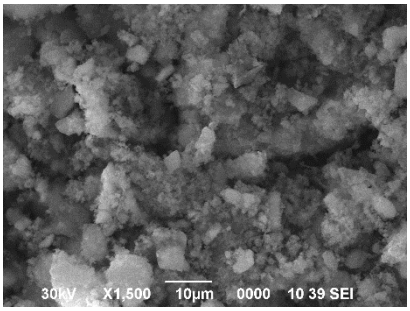

a4).

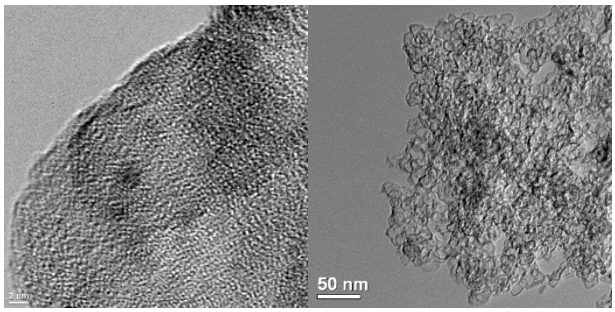

b4).

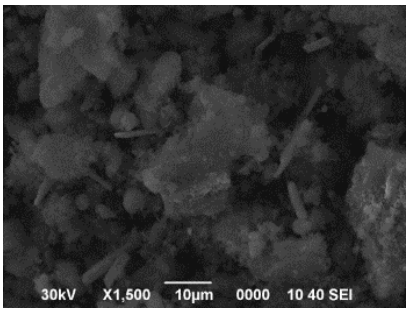

a5).

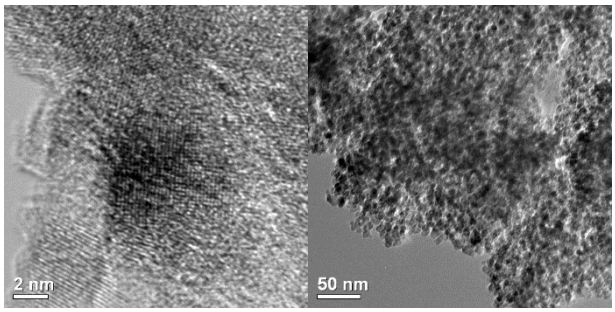
2 nm
50 nm

b5).

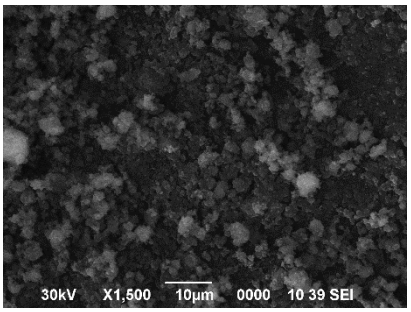
30kV X1,500 10µm 0000 10 39 SEI

a6).

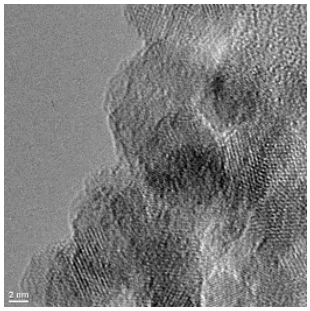

b6).

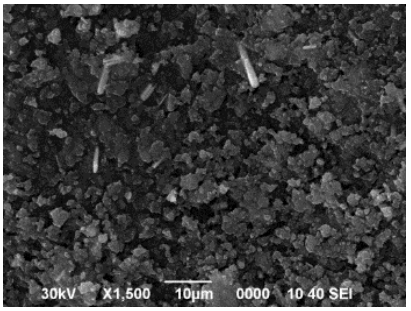
30kV X1,500 10µm 0000 10 40 SEI

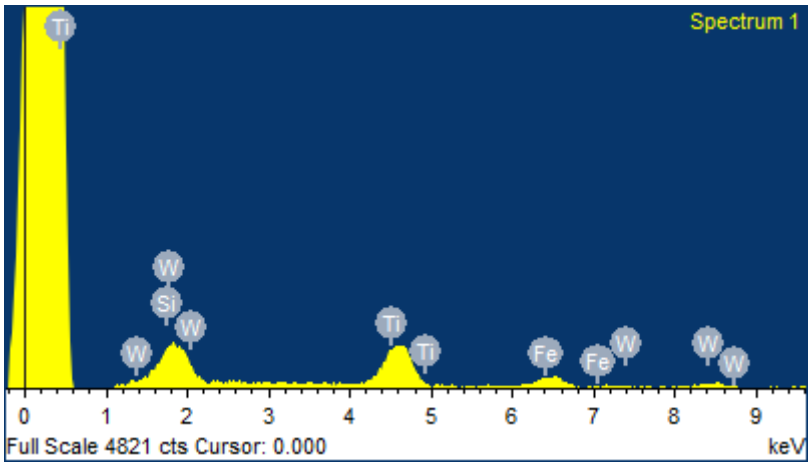
Spectrum 1
Ti
W
Si
W
W
Ti
Ti
Fe
Fe
W
W
W
0
1
2
3
4
5
6
7
8
9
Full Scale 4821 cts Cursor: 0.000
keV

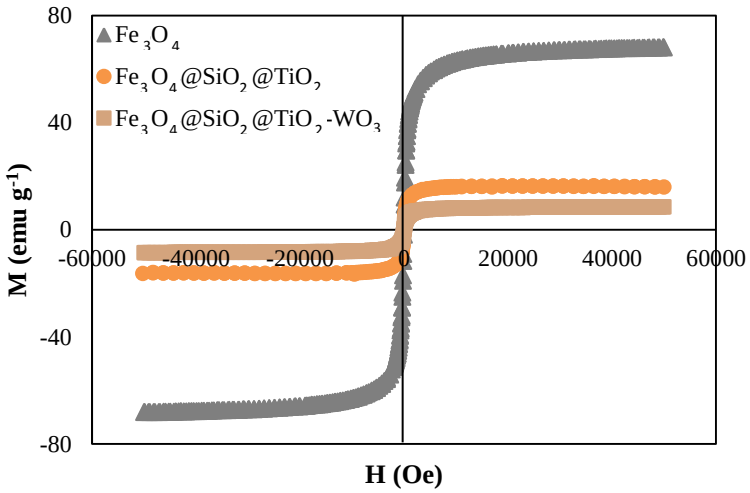
80
40
0
-40
-80
-60000
-40000
-20000
0
20000
40000
60000
Fe3O4
Fe3O4@SiO2@TiO2
Fe3O4@SiO2@TiO2-WO3
M (emu g-1)
H (Oe)

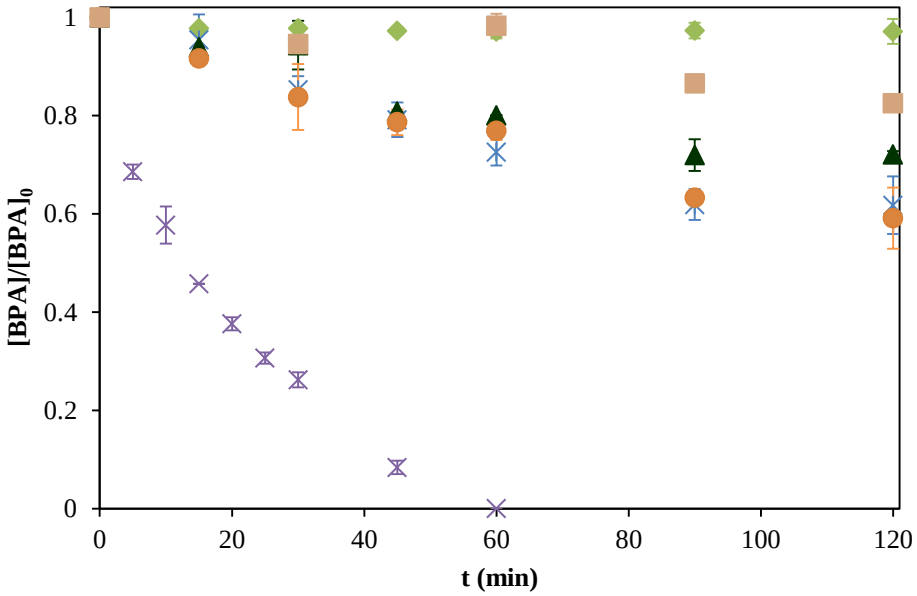
1
0.8
0.6
0.4
0.2
0
[BPA]/[BPA]0
0
20
40
60
80
100
120
t (min)

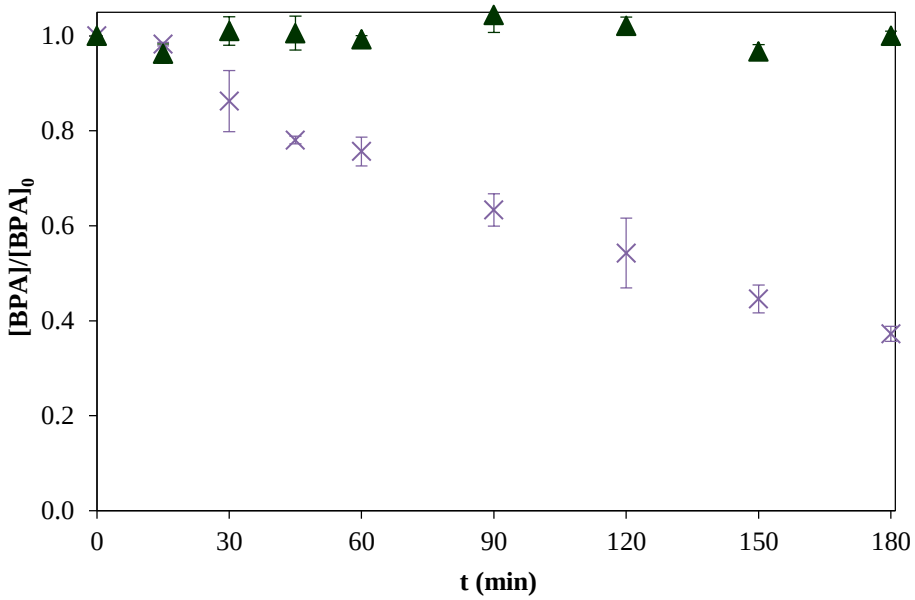
1.0
0.8
0.6
0.4
0.2
0.0
[BPA]/[BPA]0
0
30
60
90
120
150
180
t (min)

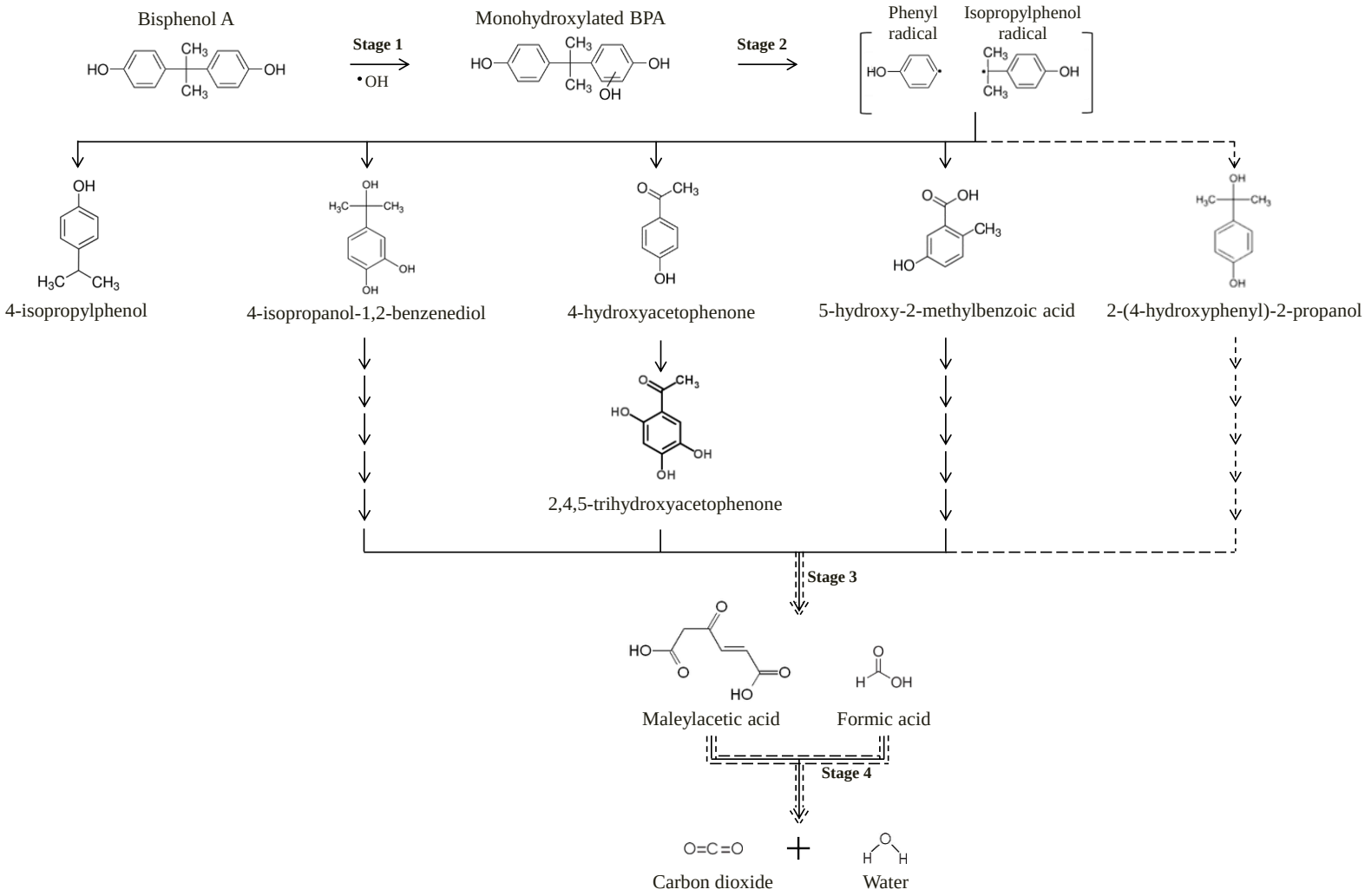
Bisphenol A
Stage 1
•OH
Monohydroxylated BPA
Stage 2
Phenyl radical
Isopropylphenol radical
4-isopropylphenol
4-isopropanol-1,2-benzenediol
4-hydroxyacetophenone
5-hydroxy-2-methylbenzoic acid
2-(4-hydroxyphenyl)-2-propanol
2,4,5-trihydroxyacetophenone
Stage 3
Maleylacetic acid
Formic acid
Stage 4
Carbon dioxide
Water